Raman Spectroscopy of Individual Single-Walled Carbon Nanotubes from Various Sources

7 AUTHORS, INCLUDING:

Frank Hennrich
Karlsruhe Institute of Technology
158 PUBLICATIONS **6,903** CITATIONS

SEE PROFILE

Ralph Krupke
Karlsruhe Institute of Technology
95 PUBLICATIONS **3,932** CITATIONS

SEE PROFILE

Daniel E Resasco
University of Oklahoma
331 PUBLICATIONS **11,029** CITATIONS

SEE PROFILE

Raman Spectroscopy of Individual Single-Walled Carbon Nanotubes from Various Sources

Frank Hennrich,*,† Ralph Krupke,† Sergei Lebedkin,† Katharina Arnold,† Regina Fischer,‡ Daniel E. Resasco,§ and Manfred M. Kappes†,‡

Forschungszentrum Karlsruhe, Institut für Nanotechnologie, D-76021 Karlsruhe, Germany, Institut für Physikalische Chemie, Universität Karlsruhe, D-76128 Karlsruhe, Germany, and School of Chemical Engineering and Materials Science, University of Oklahoma, Oklahoma 73019

Resonance Raman spectroscopy/microscopy was used to study individualized single-walled carbon nanotubes (SWNTs) both in aqueous suspensions as well as after spin-coating onto Si/SiO$_2$ surfaces. Four different SWNT materials containing nanotubes with diameters ranging from 0.7 to 1.6 nm were used. Comparison with Raman data obtained for suspensions shows that the surface does not dramatically affect the electronic properties of the deposited tubes. Raman features observed for deposited SWNTs are similar to what was measured for nanotubes directly fabricated on surfaces using chemical vapor deposition (CVD) methods. In particular, individual semiconducting tubes could be distinguished from metallic tubes by their different G-mode line shapes. It could also be shown that the high-power, short-time sonication used to generate individualized SWNT suspensions does not induce defects in great quantities. However, (additional) defects can be generated by laser irradiation of deposited SWNTs in air, thus giving rise to an increase of the D-mode intensity for even quite low power densities ($\sim$10^4 W/cm^2).

1. Introduction

Single-walled carbon nanotubes (SWNTs) are promising building blocks for nanoscale electronics due to their exceptional electronic and structural properties.[1] Their electronic structure exhibits a strong dependence on the tube diameter *d*. This diameter is uniquely related to the SWNT structure by two chiral indices *n* and *m* that define the "rollup" vector on a graphene sheet.

The successful preparation of aqueous suspensions with significant fractions of individualized SWNTs has opened new directions in carbon nanotube research,[2−5] because a "molecule-based", *n,m*-specific approach to SWNTs is now possible. Two criteria are generally used in order to infer the presence of a "large fraction" of individualized tubes in suspension. First, absorption features of such individual SWNT suspensions are much sharper compared to features of absorption spectra measured on tubes organized in bundles.[2] Second, individual semiconducting tubes also show photoluminescence (PL), and experimentally observed PL peaks can be assigned to specific tubes with specific combinations of the chiral indices *n* and *m*.[3,4]

PL of semiconducting tubes is generally thought to be quenched in bundles. Even small bundles are to first order regarded as invisible to PL. It is unclear whether this assumption is fully accurate. Luminescence quenching is likely primarily because of energy transfer to adjacent metallic tubes. Given a statistical *n,m*-abundance distribution in bundles, the probability of having a metallic tube in close proximity to the excited semiconducting SWNT becomes essentially unity for bundles containing more than four tubes. For smaller bundles without metallic tube content, one can envisage two limiting situations:

Either there is no PL quenching (energy transfer is not possible because of level mismatch), or energy transfer occurs to other PL-active semiconducting SWNTs.

Raman spectroscopy has also been intensively used to characterize SWNTs.[6] The bulk of these studies has been applied to materials characterization and has consequently been done on bundles. Some Raman investigations have also been performed on isolated tubes, in particular, on SWNTs grown on surfaces by CVD. Dresselhaus and co-workers[7,8] have comprehensively studied the basic vibrational properties of individual SWNTs in this fashion. The recent availability of individualized tube suspensions has made it possible to study the Raman spectra of isolated SWNTs in a liquid/micelle environment as well.[9−12] Telg et al. were able to obtain the optical transition energies and radial breathing-mode frequencies of $\sim$50 different types of individualized nanotubes present in the aqueous surfactant suspensions of SWNT material by recording resonance Raman excitation profiles for the ensemble.[12] Fantini et al. have recently expanded this correlation using excitation wavelength-dependent Stokes and anti-Stokes Raman spectra of aqueous SWNT suspensions.[13] Furthermore, these authors have also reported excitation profiles and red shifts for the same tube types in solid material (i.e., in the limit of large bundles). As for absorption and PL measurements, it is presently not clear how Raman excitation profiles and cross-sections differ between an individualized *n,m*-SWNT and the same *n,m*-type in a small bundle.

In a pioneering study, Hartschuh et al. have microscopically imaged fluorescence and Raman scattering simultaneously from the same SWNT spin-coated onto glass from an individual tube suspension.[14] Many sets of individual-molecule Raman and PL were acquired at various sample spots showing the same polarization dependence. Measurements on separate specimens of the same *n,m*-SWNT always manifested the same Raman spectra; however, spectrally resolved PL varied significantly in

* Frank.Hennrich@int.fzk.de.
† Institut für Nanotechnologie.
‡ Universität Karlsruhe.
§ School of Chemical Engineering and Materials Science.

both position and intensity from specimen to specimen. This was attributed to defects. However, no statistically significant sampling of PL versus Raman activity was performed, and in particular, the role of small bundles was not discussed. Such multisampling of the same *n,m*-type could provide further input into the issue of small bundles if the effect of defects can first be gauged.

Toward this goal, we are presently involved in comparative Raman/PL measurements of SWNTs on inert surfaces. Here, we report a series of Raman microscopic studies of SiO_2-deposited individualized SWNTs, focusing both on the effect of deposition as well as on the role of defects in SWNTs. The latter are in turn dependent on the production method and the sample quality. We compare several different SWNT materials of varying (but overlapping) diameter distribution. Generating suspended individual tubes from bundled material using surfactants requires strong sonication,[2] which might damage tubes by cutting and/or introducing additional defects (and also involves the presence of surfactant molecules surrounding the tubes). We explore how sonication influences Raman response for individualized SWNTs subsequently deposited onto an inert surface. Comparative PL/Raman imaging of surface-deposited SWNTs with the goal of learning about bundle content in the precursor suspension requires that deposition itself does not lead to appreciable rebundling. To gauge this, we also compare Raman spectra acquired for the ensemble of nanotubes in individualized SWNT surfactant suspensions with Raman spectra obtained for nanotubes spin-coated from these suspensions onto Si/SiO_2.

2. Experimental Section

Four different SWNT samples were studied: (i) NiY-PLV-SWNTs generated by laser vaporization[15] using a catalyst with 1 atom % Ni and Y and Ar as a carrier gas; (ii) NiCo-PLV-SWNTs with 1 atom % Ni and Co catalyst; (iii) HiPco-SWNTs from Rice University,[16] and (iv) CoMoCAT-SWNTs made using a silica-supported Co and Mo catalyst.[17]

To obtain individualized tubes in suspension, 100 mg of raw soot was sonicated for 10 min with a tip sonicator (Bandelin, 200 W, 20 kHz) in 100 mL D_2O containing 1 wt % of the surfactant sodium dodecylbenzene sulfonate (SDBS), similar to the procedure described in ref 2. The sample was not cooled, and boiling temperature was reached during sonication. After sonication, the suspensions were centrifuged at 154 000 g for 4 h, and the upper 90% of the supernatant was carefully decanted.

An otherwise analogously prepared HiPco suspension was centrifuged at only 6 000 g for 1 h in order to generate a supernatant with a higher content of bundles. After decanting, this supernatant was diluted with D_2O + 1 wt % SDBS until the tube concentration was comparable on the basis of absorption spectra (same absorbance at 300 nm) to that of the HiPco suspension which had been centrifuged with 154 000 g for 4 h.

The individualized tube suspensions were characterized by absorption, fluorescence, and Raman spectroscopy. For absorption and fluorescence, we made use of measurement setups and procedures which have already been described in ref 18. Raman spectra were acquired with a confocal Raman microscope (WiTec) with a spectral resolution of 3.75 cm^{-1} (the absolute accuracy of Raman shift determination was ca. 1 cm^{-1}) using backscattering configuration and a 100× objective (∼1 μm spot size) excited with an HeNe laser at 632.8 nm excitation with a power density of ∼3 × 10^4 W/cm^2. To prepare samples for Raman spectroscopy, a drop (∼10 μl) of suspension was spin-coated (4 000 rpm for 1 min) onto a piece (10 × 10 mm^2) of Si

wafer comprising a 600 nm thick SiO_2 surface layer and dried at room temperature. Samples were subsequently probed under ambient conditions.

In the case of the HiPco material, Raman spectra were also measured on an ensemble of individualized tubes in suspension. For this, a drop (∼10 μl) of suspension was placed onto an Si wafer, and the excitation laser was focused into the droplet. To obtain Raman spectra for isolated SWNTs on an Si/SiO_2 substrate, the laser was focused onto the substrate surface, and the sample was scanned by manually stepping the piezo table until a Raman signal was observed. Under these conditions, only those tubes for which the excitation energy matches the energy of an optically allowed interband transition are observable. For all samples measured, a sufficiently low tube (or tube bundle) density on the surface was achieved such that roughly 1 Raman active spot was observed per ∼1 μm^2. Approximately 100 Raman active spots were measured for every tube material in order to be able to draw statistically meaningful inferences. All radial breathing-mode (RBM) peak positions were obtained by Lorentzian fitting of the corresponding spectral region.

3. Results and Discussion

3.1. Background Information. *3.1.1. Electronic Structure in Single Nanotubes.* The first two interband transitions for semiconducting SWNTs, S_1 and S_2, in aqueous HiPco-SDS suspensions have been determined by means of fluorescence spectroscopy.[3] From those measurements, Weisman et al. have developed empirical fitting functions for S_1 and S_2 which have provided the basis for an empirically based Kataura plot that gives reliable predictions of optical transition energies for semiconducting SWNTs in specific aqueous surfactant suspensions under ambient conditions.[19] Recently, S_1 and S_2 interband transitions for semiconducting SWNTs and M_1 interband transitions for metallic SWNTs could be obtained by means of Raman spectroscopy on aqueous SDS suspensions of HiPco SWNTs.[12,13] Nevertheless, not all of the SWNTs possible in the diameter range probed in the present study have been comprehensively characterized by experiment. In particular, for the larger-diameter tubes, we therefore have to rely on calculations. The tight-binding description of the band structure of graphite including only nearest-neighbor interactions was intensively used to derive band structures for SWNTs.[20] Such calculations have the advantage of being inexpensive and fast. Recently, the model could be improved by Reich and co-workers by taking into account second and third nearest-neighbor interactions.[21] Also of interest in this context are recent first principles calculations on an (8, 0) tube by Spataru et al.[22] as well as extended tight-binding calculations on a variety of *n,m*-tubes by Samsonidze and co-workers.[23]

3.1.2. Raman Active Vibrations. The Raman spectrum of a single nanotube basically contains three characteristic features.[7] An RBM is found between 100 and 400 cm^{-1} for tubes with diameters between ∼0.6 and 2 nm. The RBM frequency was theoretically predicted to be dependent on the diameter $d = (3^{0.5} \cdot a_{c-c}/\pi) \cdot (n^2 + n \cdot m + m^2)^{0.5}$ of the SWNT through the relation $\omega_{RBM} = C_1/d + C_2$. These parameters have recently been empirically determined from Raman measurements for HiPco tubes in surfactant suspensions.[3,12,13] Bachilo et al. find $C_1 = 223.5$ cm^{-1} and $C_2 = 12.5$ cm^{-1} using a C−C bond distance a_{c-c} of 0.144 nm (scaling to a C−C distance of 0.142 nm yields $C_1 = 220.4$ cm^{-1} nm and $C_2 = 12.5$ cm^{-1})[3]. Telg et al. find values of $C_1 = 214$ cm^{-1} nm and $C_2 = 19$ cm^{-1} using a C−C bond distance of 0.142 nm. Fantani et al., who also used a C−C bond distance of 0.142 nm, have tabulated two

Raman Spectroscopy of SWNTs from Various Sources

J. Phys. Chem. B, Vol. 109, No. 21, 2005 **10569**

different sets of C_1 and C_2 values: for semiconducting (223 cm^{-1} nm and 10 cm^{-1}) and metallic (218 cm^{-1} nm and 17 cm^{-1}) nanotubes, respectively. The average ($C_1 = 220$ cm^{-1} nm and $C_2 = 14$ cm^{-1}) is in good agreement with Bachilo et al.[3]

The feature in the region between 1500 and 1600 cm^{-1} is related to the Raman-allowed tangential G-mode of graphite which occurs at ca. 1582 cm^{-1}. Unlike graphite, the tangential G-mode in SWNTs is a sum of up to six high-energy tangential modes that basically originate from breaking the symmetry of the tangential vibration when the graphene sheet is rolled into a tube. A simple analysis of the G-mode region can however be carried out by considering it to comprise two intense superimposed peaks. These peaks are labeled G$^+$, for atomic displacement along the tube axis, and G$^-$, for modes with atomic displacement along the circumferential direction. The line shape of the G$^-$ mode depends on whether the tube is semiconducting or metallic. The G$^-$ feature is broadened for metallic SWNTs and is usually fit using a Breit−Wigner−Fano (BWF) line in comparison with the Lorentzian line shape for semiconducting tubes.

The SWNT Raman feature around 1350 cm^{-1} is called the disorder-induced D-mode. A similar mode is observed in graphite and has recently been explained in terms of a double-resonant Raman scattering process involving a defect.[24]

Raman spectroscopy has already been used extensively to probe single nanotubes mainly grown on Si/SiO$_2$ surfaces by CVD. These studies have focused on the dependence of RBM, G- and D-mode features on nanotube diameter, and chiral angle. Correspondingly, information has been obtained on intensity, line width, and polarization properties of each such feature, with their dependence on laser excitation energy as well as data on the connection between spectra at the single nanotube level versus Raman spectra for SWNT bundles.[7]

3.1.3. Bundling Effects. Everything stated so far is valid for individual tubes. For bundles, things get more complicated. First, the above-mentioned typical Raman features become broadened by the simple fact that in a large bundle there is a convolution of peaks from several different resonant metallic and semiconducting SWNTs. Second, the electronic and vibrational properties of a single tube are affected by other surrounding tubes. From calculations, it is expected that the density of states is broadened and vHSs are shifted up to ∼100 meV as nanotubes aggregate into bundles.[25] In practice, the absorption spectrum of large nanotube bundles is red-shifted and broadened. This has been inferred by two methods: by comparing absorption spectra of individual and bundled nanotube suspensions[2] and recently in Raman studies for individualized and bundled nanotubes.[11,13] Additionally, it could be shown that no significant change in RBM frequencies occurs when going from isolated individual to large nanotube bundles.[11]

As a result of resonance shifts, we expect to be sensitive to different tube types and therefore to observe different RBM frequencies when measuring Raman spectra for large bundles versus individualized tube samples using one common excitation wavelength.

Additionally, researchers have found that the BWF line intensity for the G-mode of metallic tubes depends on the bundle thickness[26] and in particular on the relative abundance of metallic tubes in that particular bundle.

3.2. Absorption Spectroscopy − Ensembles. Figure 1 shows absorption spectra of the individual tube suspensions for all SWNT materials used in this study, after centrifugation to yield nanotube supernatant concentrations of ∼10 mg/L. All spectra show structured instead of broad unstructured absorption features
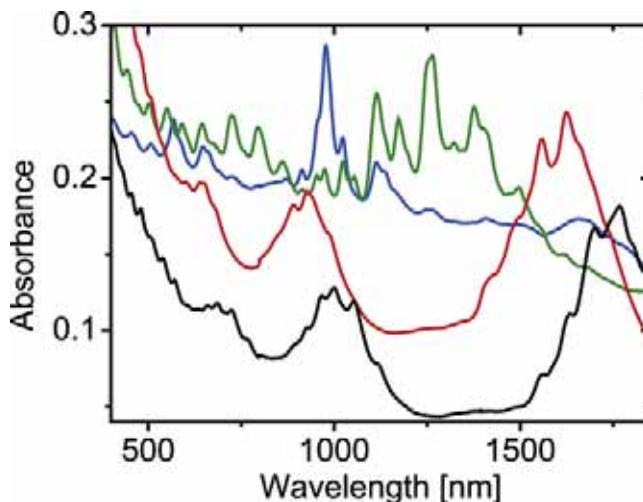

Figure 1. Absorption spectra of decant after centrifugation with 154 000 g for 4 h of tube materials used in this work: (black) NiY-PLV-SWNTs, (red) NiCo-PLV-SWNTs, (green) HiPco-SWNTs, (blue) CoMoCAT-SWNTs.

indicating that a significant fraction of tubes are suspended as individuals. Note that we also centrifuged suspensions for even longer times (up to 8 h at 154 000 g) in order to check if a further reduction in bundle content can be induced. However, apart from an overall loss of absorbance, no further sharpening or shifting of absorption features was observed in going from 4 to 8 h centrifugation.

3.3. Fluorescence Spectroscopy − Ensembles. For every SWNT material investigated in this work, so-called 2D contour plots were determined by detecting the emission spectra of semiconducting tubes for excitation at various wavelengths. Because the contour plots of the CoMoCAT-SWNTs and the HiPco tubes are very similar to the ones already published by Bachilo et al.,[3,27] we do not show them here. On the basis of the assignment of these authors, discrete peaks in these plots can be assigned in the case of the CoMoCAT-SWNTs to ∼12 distinct pairs of n and m for semiconducting tubes having diameters between ∼0.6 and 1.0 nm, whereas the (6, 5)-tube is dominant and to ∼34 distinct pairs of n and m for the HiPco tube suspensions having diameters between ∼0.7 and 1.3 nm. The contour plot of the NiCo-PLV-SWNTs is very similar to the one which was already obtained by Lebedkin et al.[18] With the assignment of Bachilo et al.,[3] ∼28 distinct pairs of n and m having diameters between ∼1.0 and 1.4 nm could be obtained.

A contour plot of the NiY-PLV-SWNTs could also be obtained but is less informative, because emission spectra can only be detected up to 1850 nm in D$_2$O due to the presence of vibrational overtones of D$_2$O in this spectral region. Nevertheless, the absorption spectrum (see Figure 1) indicates that the NiY-SWNTs-soot contains tubes with a diameter distribution between ∼1.2 and 1.6 nm.

3.4. Raman Measurements and Spectral Assignment. In most previous Raman investigations of single SWNT samples, the n,m assignment of those tubes addressed via laser excitation has required a comparison with a Kataura plot derived from calculations. In the following, we will use a Kataura plot from an improved tight-binding model[21] and an experimental Kataura plot derived from fluorescence measurements of Bachilo et al.[3] as well as from transition energies obtained from Raman measurements of Telg et al.[12] and Fantini et al.[13] We carry out this assignment for tubes from various sources spin-coated onto Si/SiO$_2$ from aqueous suspensions. Because we are using 632.8 nm = 1.96 eV as the excitation energy, the most interesting
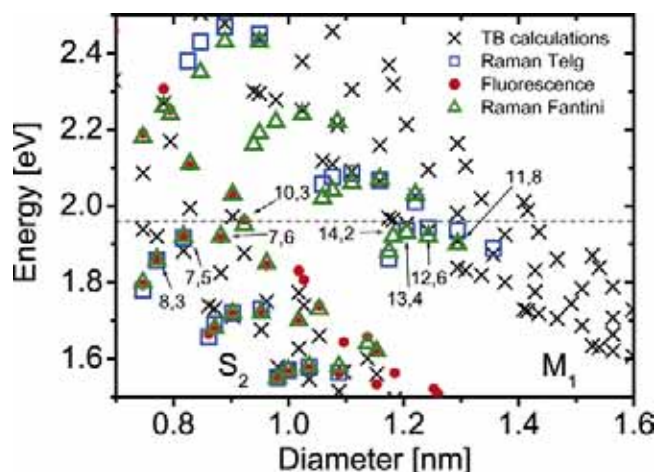
Figure 2. Kataura plot as derived from experiment and theory: from the empirical model for semiconducting tubes of Weisman et al.[19] (●), from third nearest neighbor tight-binding calculations[21] (+), and M_1 transition energies as extracted from measured Raman measurements from Telg et al.[12] (□) and Fantini et al.[13] (△) for HiPco tubes in suspension. The dashed line represents the energy of the excitation laser used in the Raman experiments. At a laser energy of $E_{exc} = 1.96$ eV, we expect semiconducting SWNTs with diameters $d < 1.1$ nm and metallic SWNTs with diameters $d > 1.1$ nm to be in resonance.

part of the Kataura plot is the region around 2.0 eV for tubes with diameters between 0.6 and 1.6 nm, as shown in Figure 2.

3.4.1. Ensemble Suspension Measurements. To establish which specific individual *n,m*-tubes we expect to see on the surface, we first measured Raman spectra for an ensemble of individualized tubes in aqueous suspension. To examine whether extensive rebundling occurs upon spin-coating, we also measured Raman spectra of suspensions which had not been strongly centrifuged in order to look for bundle-specific Raman features.

Figure 3a shows a spectrum acquired on HiPco tubes in aqueous suspension centrifuged at 6 000 g and 154 000 g. For the given diameter distribution of the HiPco material ($d \approx 0.7-$1.3 nm), we expect to hit both metallic and semiconducting tubes at the excitation energy of 1.96 eV. The G-mode region is dominated by a sharp G^+ peak. The features in the RBM region in the case of the suspension centrifuged with 154 000 g could be fitted with at least five Lorentzian functions with peak positions (fwhm) of 190 (14) cm^{-1}, 196 (7) cm^{-1}, 253 (8) cm^{-1}, 265 (6) cm^{-1}, and 283 (8) cm^{-1}, which can be assigned following Figure 2 to metallic tubes (12, 6) and (13, 4) and semiconducting tubes (10, 3), (7, 6), and (7,5), respectively. We have elected to fit the broad feature at around 195 cm^{-1} with two peaks, but a fit with more than two features is also possible.

We assume that the suspension centrifuged at 6 000 g comprises mainly bundled tubes. Bundling causes red-shifting and broadening of the interband transitions, as was shown recently by O'Connell and co-workers[11] and Fantani and co-workers.[13] We therefore expect to obtain different resonant tube types and different RBM frequencies when measuring Raman spectra for bundled versus individualized tubes. Figure 3b shows the RBM frequency region of the spectra acquired for HiPco tubes in aqueous suspension centrifuged at 6 000 g and 154 000 g. The most noticeable difference is the strong presence of the 218 cm^{-1} RBM frequency in the bundled tubes sample, absent in the individualized nanotubes sample. This peak can be used as an indicator for bundles in a sample.

It has been speculated that intensive sonication might damage tubes by cutting and/or introducing defects which should be visible by correspondingly large D-mode intensities. These could
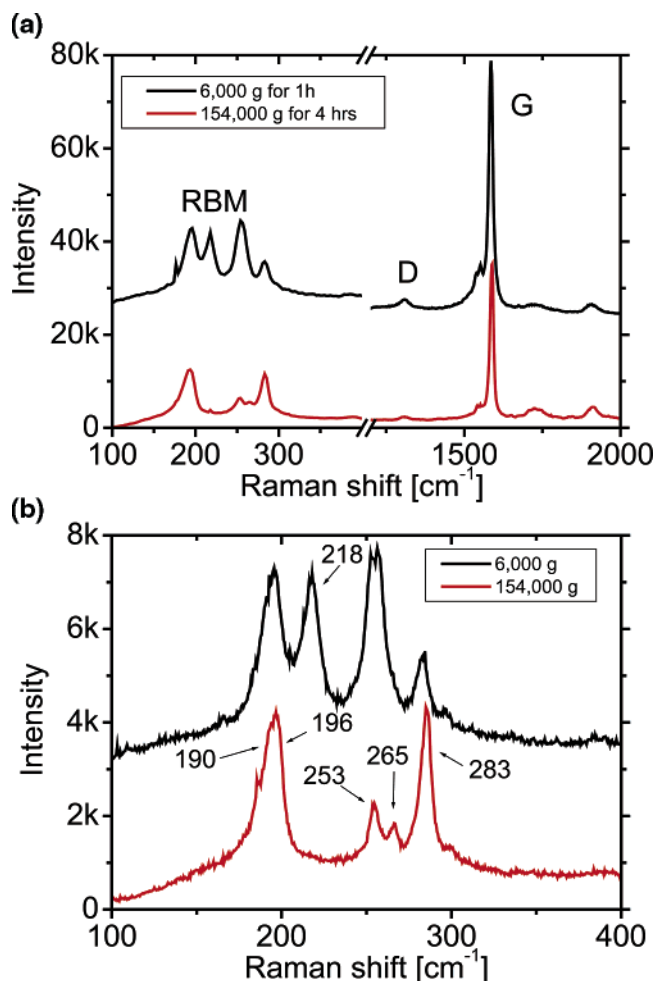

Figure 3. (a) Raman spectrum of a HiPco SWNTs suspension after centrifugation at 6.000 g for 1 h and after centrifugation at 154 000 g for 4 h. (b) RBM frequency region.

not be detected for the individual HiPco-SWNT suspensions here (not shown). Note, however, that recent Raman measurements on nanographitic ribbons have shown that specific defect types may not be D-band active.[28]

3.4.2. Raman Microscopy of HiPco SWNTs on Si/SiO$_2$. 3.4.2.1. Statistics and Surface Interaction. Approximately 100 Raman active spots were measured for every tube material spin-coated onto Si/SiO$_2$. In the case of the HiPco material, ~50 of these active spots showed a G-band but no measurable RBM mode(s). Approximately 40 of the Raman active spots showed only 1 RBM frequency. We interpret each of the latter spectra as due to one individual SWNT. Note, however, that with resonance Raman alone it is not possible to distinguish whether we are measuring only one SWNT or perhaps a very small bundle also comprising nonresonant tube(s). Typical spectra corresponding to six different Raman active spots showing RBM intensity are presented in Figure 4a,b. Of these, 3 show a very broad G-mode and will therefore be considered to be deriving from metallic nanotubes, and 3 show a very intense sharp G-mode and will therefore be considered to be deriving from semiconducting nanotubes. In the case of the metallic nanotubes, the G-mode is much less intense than the RBM features. The RBM peak positions (fwhm/frequency of occurrence) could be determined to 190 (10/3) cm^{-1}, 196 (9/5) cm^{-1}, and 198 (10/3) cm^{-1} in the case of the metallic nanotubes and to 254 (12/5) cm^{-1}, 258 (11/2) cm^{-1}, and 284 (11/4) cm^{-1} in the case of the semiconducting nanotubes. This is quite similar to what we observed in the ensemble measurements of the nanotubes in

suspension. The only significant difference is the observation of a nanotube with an RBM frequency of 258 cm⁻¹ instead of 266 cm⁻¹. This feature could conceivably be assigned to the (11, 1) tube, which is the next closest of the empirically assigned tubes to 1.96 eV (see Figure 2). From that, we conclude that we excite the same nanotubes both in suspension and on Si/SiO₂ surfaces. Furthermore, we conclude that the RBM vibrational properties of the nanotubes are not altered when spin-coated on Si/SiO₂. Similarly, changes of the electronic structure due to interaction with the surface are such that overall shifts in S_2 and M_1 transition energies are less than the experimental resonance window in solution (ca. 60 meV). Recently, Htoon and co-workers drew a similar conclusion concerning the interaction of SWNTs with surfaces.[29] They measured photoluminescence for HiPco tubes spin-coated onto Si/SiO₂ from suspensions and for ensembles of individualized tubes in suspensions, indicating that the surface does not affect the electronic properties of tubes.

3.4.2.2. Bundles. We now come back to the issue of whether we investigated individual tubes or small bundles. From the Raman measurements on bundled tubes in suspensions (see above), we know that we probe some different tube types than in individualized samples because of different resonance conditions.[11,13] The most noticeable difference for the HiPco material under our conditions is the strong presence of the 218 cm⁻¹ RBM frequency in the bundled tubes sample. For the individualized tubes on the Si/SiO₂ surface, we were never able to detect the 218 cm⁻¹ RBM frequency indicating the absence of large bundles in the 40 RBM active spots characterized. Consequently, it appears that no significant rebundling occurs on the surface under our spin-coating conditions.

For control purposes, we also spin-coated HiPco suspensions containing SWNT bundles onto Si/SiO₂ (under comparable conditions to those used for individualized suspensions). Of the 100 Raman active spots measured for this sample, 82 showed two or more RBM frequencies. Of these 82, 20 RBM regions contained the 218 cm⁻¹ RBM frequency indicating the presence of bundles on the surface. In 5 cases, the 218 cm⁻¹ RBM frequency dominates the RBM frequency region, indicating the presence of a quite small bundle where mainly the tube with the 218 cm⁻¹ RBM frequency is in resonance with the excitation wavelength. Figure 4b includes the measurement of such a small bundle (blue curve). On the basis of the empirical Kataura plot for bundled tubes from the work of Fantini et al.,[13] we assign this tube to a (12, 3)-tube.

3.4.2.3. Defects. When measuring isolated tubes, the smallest laser power density possible was used to prevent damaging the tubes. Damage could easily be followed by the change of the D-mode intensity with time. Below a certain power density threshold, which was observed to be diameter dependent (larger diameters having larger thresholds), tubes were observed to be stable under laser irradiation for minutes or even longer (i.e., no change in the D-mode intensity). Above this threshold, the D-mode intensity increases with time during irradiation. In particular, for the smallest diameter tubes present, even very low power densities (~10⁴ W/cm²), close to the detection limit, appeared to lead to some measurable destruction (oxidation?).

For HiPco samples, 632.8 nm excitation probe semiconducting tubes with $d < 1.1$ nm and metallic tubes with $d > 1.1$ nm. In statistical measurements at the same power density, the semiconducting tubes showed significant D-mode intensity, whereas the metallic tubes were essentially Raman silent at this Stokes shift. This is again consistent with the inference that smaller-diameter tubes are more sensitive to destruction due to
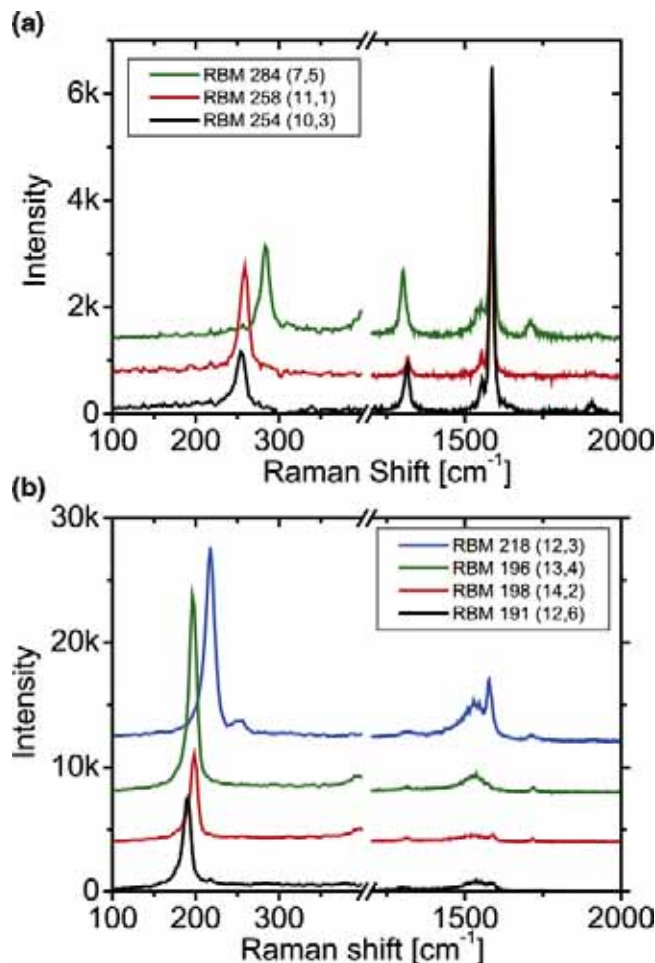

Figure 4. (a) Raman spectra of isolated semiconducting HiPco SWNTs and (b) isolated metallic HiPco SWNTs and one small bundle (blue) spin-coated onto Si/SiO₂.

laser irradiation (assuming that the absorption cross-sections and the thermal conductivity of small- and larger-diameter nanotubes are not much different).

D-mode intensity is regarded as a measure for defect density.[24] Going above the threshold irradiation apparently induces defects. Because Raman spectra were obtained in air, the tubes could simply be oxidized while being laser-heated. Smaller-diameter tubes are known to be more sensitive toward oxidation because of stronger curvature. For example, smaller-diameter SWNTs are more rapidly etched away upon being treated with nitric acid.[30] We speculate that D-mode active defects might correspond to open tube ends and sidewall holes. Note that Raman spectra taken for the same small-diameter tubes in suspension (see Figure 3) have a significantly lower D-mode intensity, probably because deposited heat can be conducted away by D₂O, and therefore, tube temperatures remain lower than those on surfaces (and consequently, oxidation is precluded).

3.4.3. CoMoCAT-SWNTs on Si/SiO₂. Figure 5 shows four Raman spectra obtained on CoMoCAT-SWNTs spin-coated onto Si/SiO₂. Because the CoMoCAT material has a diameter distribution between ~0.6−1.0 nm, we expect to detect only semiconducting tubes when exciting with 632.8 nm (see also Figure 2 for comparison). Indeed, while scanning over the sample, four different Raman spectra with very intense sharp G-mode features could be found, having RBM peak positions (fwhm/frequency of occurrence) of 255 (12/2) cm⁻¹, 266 (9/2) cm⁻¹, 284 (12/14) cm⁻¹, and 301 (10/3) cm⁻¹. No metallic tubes
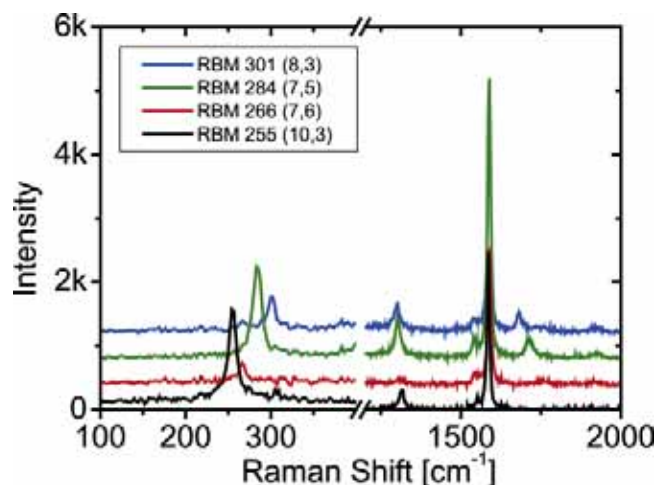
Figure 5. Raman spectra of isolated semiconducting CoMoCAT-SWNTs spin-coated onto Si/SiO$_2$.
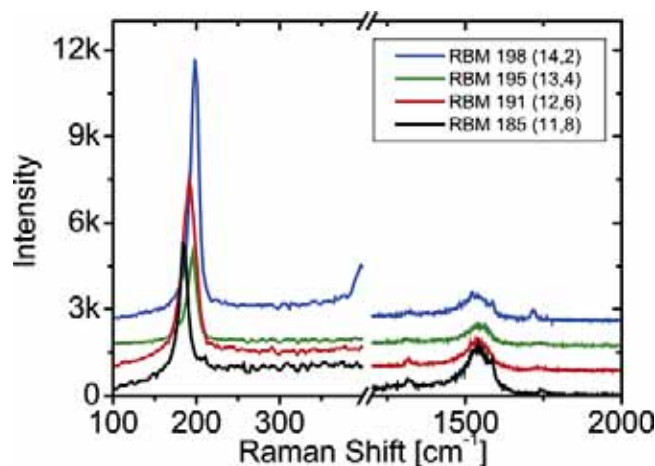

Figure 6. Raman spectra of isolated metallic NiCo-PLV-SWNTs spin-coated onto Si/SiO$_2$.

were observable in the corresponding scan area. The observed RBM frequencies are within 1 cm^{-1} of our findings for surface-deposited HiPco material with the exception of one smaller tube having 301 cm^{-1}. This has been assigned as an (8, 3) tube.

3.4.4. NiCo-PLV-SWNTs on Si/SiO$_2$. For the NiCo-PLV material, we expect to excite only metallic tubes, because they have diameters between ∼1.0 and 1.4 nm (see Figure 2). Figure 6 shows four Raman spectra with different RBM frequencies obtained on isolated NiCo-PLV-SWNTs spin-coated onto Si/SiO$_2$. All spectra show very broad G-mode features indicating metallic character with intensities smaller than the corresponding RBM intensities, similar to what was detected for the metallic tubes in HiPco material. RBM peak positions (fwhm/frequency of occurrence) could be located at 185 (12/11) cm^{-1}, 191 (16/10) cm^{-1}, 195 (13/8) cm^{-1}, and 198 (11/5) cm^{-1}. This is within 1 cm^{-1} of our findings for HiPco material, with the exception of one larger tube which has been assigned as the (11, 8) tube.

3.4.5. NiY-PLV-SWNTs on Si/SiO$_2$. For the NiY-PLV-SWNTs having diameters between ∼1.2 and 1.6 nm, we could detect metallic tubes with smaller RBM frequencies than for all other SWNT materials previously discussed. Figure 7 shows six different Raman spectra obtained on isolated NiY-PLV-SWNTs spin-coated onto Si/SiO$_2$. All spectra show very broad G-mode features indicating metallic character with intensities smaller than the corresponding RBM intensities, similar to what was detected for the HiPco and the NiCo material. RBM peak positions (fwhm/frequency of occurrence) could be identified
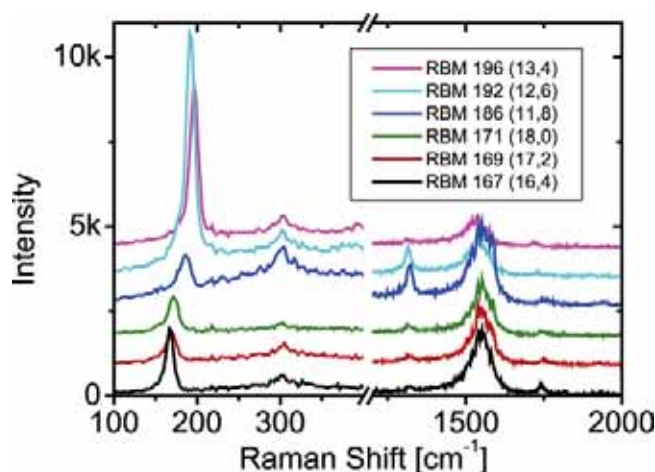

Figure 7. Raman spectra of isolated metallic NiY-PLV-SWNTs spin-coated onto Si/SiO$_2$.

TABLE 1: Summary of Observed Raman Radial Breathing-Mode Frequencies, Averaged Line Widths (fwhm), Best Assignment, and Calculated Diameter

RBM [cm^{-1}]	fwhm	assignment	d^a [nm]
167	10	(16, 4)	1.44
169	14	(17, 2)	1.42
171	14	(18, 0)	1.41
186	14	(11, 8)	1.29
191	13	(12, 6)	1.24
196	11	(13, 4)	1.21
198	11	(14, 2)	1.18
254	12	(10, 3)	0.92
258	11	(11, 1)	0.90
266	9	(7, 6)	0.88
284	12	(7, 5)	0.82
301	10	(8, 3)	0.77

^{a} $a_{c-c} = 0.142$ nm.

as 167 (10/10) cm^{-1}, 169 (14/5) cm^{-1}, 171 (14/2) cm^{-1}, 186 (15/2) cm^{-1}, 192 (12/2) cm^{-1}, and 196 (12/2) cm^{-1}. This is within 1 cm^{-1} of the findings for the NiCo material, with the exception of three larger tubes which can be assigned to the (16, 4), (17, 2), and (18, 0) tube.

3.4.6. RBM Diameter Dependence and Line Widths. Table 1 summarizes the experimentally obtained RBM frequencies, averaged line widths (fwhm), best assignment, and diameters of the twelve different kinds of isolated SWNTs found for the four different SWNT materials spin-coated onto Si/SiO$_2$. For a number of tubes, attribution of the chiral vector was equivocal, leading to several possible assignments. Our best assignment corresponds to that which yields the smallest errors for C_1 and C_2 in the linear relationship $\omega_{RBM} = C_1/d + C_2$. The corresponding values for the parameters were $C_1 = 223 \pm 2$ cm^{-1} nm and $C_2 = 12 \pm 2$ cm^{-1}, in agreement with previous work within the resolution of the spectrometer.[3,13]

The RBM line widths obtained in our study were observed to be between 9 and 14 cm^{-1} and are comparable to what other researchers have already obtained, which is somewhat larger than the experimental resolution.[31] At least in this work, when probing tubes with diameters between ∼0.7 and 1.5 nm from different sources, significant differences in line widths could not be detected (at slightly higher than room-temperature sample excitation).

4. Summary

In summary, the Raman measurements acquired on individualized SWNTs from different sources spin-coated onto Si/SiO$_2$ give rise to several conclusions.

Raman Spectroscopy of SWNTs from Various Sources

J. Phys. Chem. B, Vol. 109, No. 21, 2005 **10573**

1. It is possible to generate suspensions of all tube materials tested so as to comprise a large fraction of individualized tubes. However, the content of bundles in these suspensions after centrifugation at 154 000 g for 4 h is still unclear.

2. HiPco tubes from such individualized tube suspensions can be spin-coated onto Si/SiO$_2$ such that large bundles do not reform on the surface, as evidenced by the absence of a "bundle peak" in the corresponding Raman measurements.

3. Observed Raman features are similar to what was measured for tubes directly fabricated on surfaces (i.e., without surfactants). Semiconducting tubes could be distinguished from metallic tubes because of their different G-mode line shapes. We obtained large differences of the RBM/G-mode intensity ratios between semiconducting and metallic tubes, which has not been investigated in detail in the literature so far. Additionally, we conclude that residual surfactant does not significantly influence the Raman measurements.

4. As a result of the comparison between Raman spectra taken on HiPco tubes in suspension and on the surface, we conclude that the surface does not dramatically affect the electronic properties of SWNTs visible in Raman spectra. RBM frequencies found in suspension and on the surface were the same within the resolution of the spectrometer.

5. The D-mode analysis suggests that high-power, short-time (up to 10 min.) sonication does not induce D-mode active defects in great quantities. Similar D-mode intensities were detected for unprocessed tubes directly fabricated on surfaces.[7] Conceivably, tubes always have a natural defect density dependent on or even independent of the synthesis method. One might speculate that tube ends themselves could be regarded as such natural D-mode defects.

6. Defects can be induced by laser irradiation in air (i.e., of deposited tubes) giving rise to an increase of the D-mode intensity for even quite low power densities (~10^4 W/cm^2). While the underlying mechanism is unclear, this observation provides additional evidence that the D-mode intensity is dependent on defect density.

References and Notes

(1) McEuen, *Phys. World* **2000**, *13*, 26−31.

(2) O'Connell, M. J.; Bachilo, S. M.; Huffman, C. B.; Moore, V. C.; Strano, M. S.; Haroz, E. H.; Rialon, K. L.; Boul, P. J.; Noon, W. H.; Kittrell, C.; Ma, J.; Hauge, R. H.; Weisman, R. B.; Smalley, R. E. *Science* **2002**, *297*, 593−596.

(3) Bachilo, S. M.; Strano, M. S.; Kittrell, C.; Hauge, R. H.; Smalley, R. E.; Weisman, R. B. *Science* **2002**, *298*, 2361−2365.

(4) Lebedkin, S.; Hennrich, F.; Skipa, T.; Kappes, M. M. *J. Phys. Chem. B* **2003**, *107*, 1949−1956.

(5) Krupke, R.; Hennrich, F.; v. Löhneysen, H.; Kappes, M. M. *Science* **2003**, *301*, 344−347.

(6) Reich, S.; Thomsen, C.; Maultzsch, J. *Carbon Nanotubes*; WILEY−VCH Verlag GmbH & Co. KGaA: Weinheim, 2004.

(7) Dresselhaus, M. S.; Dresselhaus, G.; Jorio, A.; Souza Filho, A. G.; Saito, R. *Carbon* **2002**, *40*, 2043−2061.

(8) Filho, A. G.; Chou, S. G.; Samsonidze, G. G.; Dresselhaus, G.; Dresselhaus, M. S.; An, L.; Liu, J.; Swan, A. K.; Ünlü, M. S.; Goldberg, B. B.; Jorio, A.; Grüneis, A.; Saito, R. *Phys. Rev. B* **2004**, *69*, 115428.1−115428.7.

(9) Strano, M. S.; Doorn, S. K.; Haroz, E. H.; Kittrell, C.; Hauge, R. H.; Smalley, R. E. *Nano Lett.* **2003**, *3*, 1091−1096.

(10) Doorn, S. K.; Heller, D. A.; Barone, P. W.; Usrey, M. L.; Strano, M. S. *Appl. Phys. A* **2004**, *78*, 1147−1155.

(11) O'Connell, M. J.; Sivaram, S.; Doorn, S. K. *Phys. Rev. B* **2004**, *69*, 235415.1−23415.15.

(12) Telg, H.; Maultzsch, J.; Reich, S.; Hennrich, F.; Thomsen, C. *Phys. Rev. Lett.* **2004**, *93*, 177401.1−177401.4.

(13) Fantini, C.; Jorio, A.; Souza, M.; Strano, M. S.; Dresselhaus, M. S.; Pimenta, M. A. *Phys. Rev. Lett.* **2004**, *93*, 147406.1−147406.4.

(14) Hartschuh, A.; Pedrosa, H. N.; Novotny, N. *Science* **2003**, *301*, 1354−1356.

(15) Lebedkin, S.; Schweiss, P.; Renker, B.; Malik, S.; Hennrich, F.; Neumaier, M.; Stoermer, C.; Kappes, M. M. *Carbon* **2002**, *40*, 417−423.

(16) Nikolaev, P.; Bronikowski, M. J. R.; Bradley, K.; Rohmund, F.; Colbert, D. T.; Smith, K. A.; Smalley, R. E. *Chem. Phys. Lett.* **1999**, *313*, 91−97.

(17) Alvarez, W. E.; Pompeo, F.; Herrera, J. E.; Balzano, L.; Resasco, D. E. *Chem. Mater.* **2002**, *14*, 1853−1858.

(18) Lebedkin, S.; Arnold, K.; Hennrich, F.; Krupke, R.; Renker, B.; Kappes, M. M. *New J. Phys.* **2003**, *5*, 140.1−140.11.

(19) Weisman, R. B.; Bachilo, S. M. *Nano Lett.* **2003**, *3*, 1235−1238.

(20) Saito, R.; Dresselhaus, G.; Dresselhaus, M. S. *Physical properties of carbon nanotubes*; Imperial College Press: London, 1998.

(21) Reich, S.; Maultzsch, J.; Thomsen, C. *Phys. Rev. B* **2002**, *66*, 035412.1−025412.5.

(22) Spataru, C. D.; Ismail-Beigi, S.; Benedict, L. X.; Louie, S. G. *Phys. Rev. Lett.* **2004**, *92*, 077402.1−077402.4.

(23) Jorio, A.; Fantini, C.; Pimenta, M. A.; Capaz, R. B.; Samsonidze, Ge. G.; Dresselhaus, G.; Dresselhaus, M. S.; Jiang, J.; Kobayashi, N.; Grüneis, A.; Saito, R. *Phys. Rev. B* **2005**, *71*, 075401.11.

(24) Thomsen, C.; Reich, S. *Phys. Rev. Lett.* **2000**, *85*, 5214−5217.

(25) Reich, S.; Thomsen, C.; Ordejón, P. *Phys. Rev. B* **2002**, *65*, 155411.1−155411.11.

(26) Jiang, C.; Kempa, K.; Zhao, J.; Schlecht, U.; Kolb, U.; Basché, T.; Burghard, M.; Mews, A. *Phys. Rev. B* **2002**, *66*, 161404.1−161404.4.

(27) Bachilo, S. M.; Balzano, L.; Herrera, J. E.; Pompeo, F.; Resasco, D. E.; Weisman, R. B. *J. Am. Chem. Soc.* **2003**, *125*, 11186−11187.

(28) Cancado, L. G.; Pimenta, M. A.; Neves, B. R. A.; Medeiros-Ribeiro, G.; Enoki, T.; Kobayashi, Y.; Takai, K.; Fukui, K.; Dresselhaus, M. S.; Saito, R.; Jorio, A. *Phys. Rev. Lett.* **2004**, *93*, 047403.1−047403.4.

(29) Htoon, H.; O'Connell, M. J.; Cox, P. J.; Doorn, S. K.; Klimov, V. I. *Phys. Rev. Lett.* **2004**, *93*, 027401.1−027401.4.

(30) Hennrich, F.; Wellmann, R.; Malik, S.; Lebedkin, S.; Kappes, M. M. *Phys. Chem. Chem. Phys.* **2003**, *5*, 178−183.

(31) Jorio, A.; Fantini, C.; Dantas, M. S. S.; Pimenta, M. A.; Souza Filho, A. G.; Samsonidze, Ge. G.; Brar, V. W.; Dresselhaus, G.; Dresselhaus, M. S.; Swan, A. K.; Ünlü, M. S.; Goldberg, B. B.; Saito, R. *Phys. Rev. B* **2002**, *66*, 115411.1−115411.8.